

# Validating the MISR radiometric scale for the ocean aerosol science communities

Carol J. Bruegge, Wedad Abdou, David J. Diner, Barbara J. Gaitley, Mark Helmlinger, Ralph A. Kahn, and John V. Martonchik

*Jet Propulsion Laboratory, California Institute of Technology, Pasadena, California*

**ABSTRACT:** The Multi-angle Imaging SpectroRadiometer (MISR) is one of five instruments on-board the EOS/Terra spacecraft. This multi-angle capability is provided by nine cameras, which view up to 70° forward and aft of the spacecraft track and enable unique geophysical retrievals. As an example, many on-orbit sensors are able to estimate the amount aerosol loading present in the underlying atmosphere. MISR, however, is capable of retrieving both aerosol amount and aerosol compositional information. A necessary prerequisite for these retrievals is that the instrument be calibrated to its absolute, band, and camera-relative specifications. Previous work has demonstrated that MISR is calibrated to better than 4% absolute uncertainty (1 $\sigma$  confidence level) for bright land targets. This paper validates that radiometric accuracy is maintained throughout the dynamic range of the instrument. As part of this study, a new look has been taken on the band-relative scale, and a decrease in the radiance reported for the Red and NIR Bands has resulted. The calibration processes is now routine, fully developed, and tested. Bi-monthly experiments will be conducted throughout the life of the mission and allow MISR to accurately report incident radiances, even in the presence of expected sensor response changes.

## I. INTRODUCTION

### *1.1 Science drivers to accurate radiometry*

The Multi-angle Imaging SpectroRadiometer (MISR) (Diner et al. 1998) is one of five instruments on-board NASA's Earth Observing System (EOS). Data products include cloud classification parameters and albedos, wind speed and direction, surface bi-directional reflectances, and aerosol products. (Aerosols are solid or liquid airborne particulates of various compositions.) These measurements are routinely provided over the globe, and are important in the understanding of the Earth's radiation budget and climate change predictors.

One unique contribution that can be made by MISR is providing aerosol products with improved accuracies and with some degree of distinguishability. Calibration accuracy is particularly important for such aerosol retrievals over dark ocean targets. Kahn et al. (2001, 1998) provide a clear statement of the MISR aerosol science objective for such conditions. "We desire to retrieve column optical depth from measurements over calm ocean for all but the darkest particles, with typical size distributions and compositions, to an uncertainty of at most 0.05 or 20%, which ever is larger, even if the particle properties are poorly known. The measurements should also allow us to distinguish spherical from nonspherical particles, to separate two to four compositional groups based on indices of refraction, and to identify three to four distinct size

groups between 0.1 and 2.0  $\mu\text{m}$  characteristic radius at most latitudes." These expectations are based upon the theoretical studies which are documented in the cited publications. To achieve this goal in practice requires accurate top-of-atmosphere radiances for these low-light conditions.

Top-of-atmosphere (TOA) equivalent reflectance is defined here as  $\rho_{\text{toa}} = (\pi L/E_0)$ , where  $L$  is the top-of-atmosphere radiance within a given MISR band, and  $E_0$  is the MISR total-band weighted exo-atmosphere solar irradiance. Very low light levels, in the equivalent reflectance range below 7%, are typically found over dark water scenes having aerosol burdens on the order 0.2 or less at mid-visible wavelengths. Here the desired MISR radiometric calibration accuracy is at the cutting edge of current capabilities. The needed constraint amounts to  $\Delta\rho_{\text{toa}} = 0.002$  or better, for equivalent reflectance below 0.02, in all channels. This translates to a 10% absolute uncertainty at a scene equivalent reflectance of 0.02.

MISR calibration requirements for bright targets ( $\rho_{\text{eq}}=1$ ) include a 3% absolute, and 1% band and camera-relative calibrations. MISR radiometric accuracy has previously been documented (Bruegge et al. 2002, Chrien et al. 2002, Abdou et al. 2002) for bright land targets. Here vicarious calibration (VC) experiments, in conjunction with sensor cross-comparison studies and on-board-calibrator error assessments, have demonstrated that MISR radiances are uncertain to within 4% (1 $\sigma$ ) - for targets which fall

mid-range in the sensor's dynamic range. Vicarious calibration experiments are intensive field campaigns, located at uniform desert sites such as Railroad Valley, Nevada. These are conducted annually for MISR, by the Jet Propulsion Laboratory (JPL) staff. Unique tools for this JPL operation include AirMISR, a ER-2 based aircraft prototype for MISR, as well as the PARABOLA instrument, a surface based radiometer which measures upwelling and downwelling radiance in 5° samplings. For these desert VC experiments the surface reflectance term dominates the top-of-atmosphere radiance. Under clear sky, low aerosol conditions, typical for these southwest sites, top-of-atmosphere radiances are measured within an uncertainty of 3%. Vicarious calibrations are used to validate the radiometric scale of some sensors. In the case of MISR, the June 2000 vicarious campaign was used to calibrate the on-board-calibrator, which in turn scales (that is, produces radiometric gain coefficients) of the cameras on a bi-monthly basis.

Validation of MISR radiometry over dark ocean sites has added importance in that instrument artifacts, such as additive stray-light or electronic biases, if present, would lead to large radiometric errors in the measure of incident radiance. These could be as large or larger than the actual top-of-atmosphere radiance to be measured. Despite its importance, validation of MISR radiometry over dark ocean sites is more challenging than over land targets. Although dark water vicarious calibrations can be conducted, they are not routine. For these cases the atmospheric contribution to top-of-atmosphere radiance dominates over the surface term, and the process of computing top-of-atmosphere radiances from in-situ measurements is less certain. Cross-comparisons with other sensors provide an alternate validation approach. The Moderate-Resolution Imaging Spectroradiometer (MODIS) instrument is an ideal cross-comparison source. Co-located on the same platform, MODIS and MISR view a scene simultaneous in time and with similar bandpasses. Unfortunately ocean images acquired by nadir-viewing sensors, such as MODIS, are frequently contaminated with ocean glint. The large radiance gradient of these scenes makes data comparisons less reliable.

Despite the challenges encountered with the dark water validations, MISR feels that sufficient work has been done to demonstrate that its radiometric accuracy requirements are being met for homogeneous dark ocean scenes. The validation of MISR radiometry over dark targets has proceeded with all proposed approaches: 1) an error-tree analysis of the potential contributors to low-light errors, 2) cross-comparisons with MODIS scenes, 3) use of a lunar calibration experiment, and 4) dark water vicarious calibrations.

The first three of these topics are covered in this publication.

A dark-target calibration of MISR has been reported on in Kahn et al. (2004). Here data from the Aerosol Robotic Network (AERONET), in conjunction with an ocean reflectance model, are used to predict top-of-atmosphere radiances, and compared to MISR and MODIS. AERONET-based radiances are found to be systematically lower than MISR, by about 10%. MISR and the MODIS ocean channels are found to agree within 3%, with MSR reporting higher radiances. These results are consistent with the finding reported in this publication, and demonstrates that the ocean reported radiances are valid and accurate. [*Ralph: check these numbers*]

Likewise, the validation of MISR radiometry over very bright targets, such as clouds, have been reported elsewhere (Marchand, 2004; Horvath et al. 2004). These latter references support the conclusion that MISR is well calibrated, for homogeneous targets, over its entire dynamic range. [*Roger M. and Akos: provide words and references*]

## 1.2 The MISR instrument

MISR produces global data sets at nine day intervals or less, depending on latitude. The effective center wavelengths, given in Table 1, have been computed using a moments (centroid) analysis within the region delimited by the 1% response points (Bruegge et al., 2002). The effective bandwidths are also given; these parameters are used to define an equivalent square-band response function for the sensor. Approximately 3% of the camera output comes from signals at wavelengths outside these limits, for a spectrally neutral scene. Each of the nine cameras has a unique name, and is associated with a specific view angle. The cameras view a target consecutively in the order Df (70.5° fore), Cf (60.0°), Bf (45.6°), Af (26.1°), An (nadir), Aa (26.1° aft), Ba (45.6°), Ca (60.0°), and Da (70.5°), with 7 minutes from first to last acquisition of a target. Here the first letter of the camera name refers to the lens design and the second designates either the fore-, nadir-, or aft-view directions with respect to the spacecraft track. MISR has 14-bit quantization, and therefore has roughly 16,384 gray levels (the finite video offset and square-root encoding reduces this by about 300 counts). A signal of  $\rho_{\text{toa}}=0.02$  results in an output DN of from 300 to 800 DN, depending on the detector. For dark targets, errors of 30 DN may begin to affect radiometric accuracy.

Table 1. MISR in-band spectral parameters

| $\lambda_c$ , nm | $\delta\lambda$ , nm | $E_{0,b}$ [ $\text{W m}^{-2} \mu\text{m}^{-1}$ ] |
|------------------|----------------------|--|
| 447              | 41                   | 1871   |
| 558              | 27                   | 1851   |
| 672              | 20                   | 1525   |
| 867              | 38                   | 969.6  |

MISR cameras acquire data in a pushbroom configuration, using the spacecraft motion to build up an image from each of the 36 charge-coupled device (CCD) linear arrays. The spatial resolution of the MISR cameras, established by the size of the detector elements, optical focal length, and spacecraft altitude, is 275 m cross-track (for the off-nadir cameras), or 250 m (for the nadir viewing camera). Downtrack instantaneous field-of-view increases due to the view angle effects, ranging from 214 m in the nadir to 707 m at the most oblique angle. Downtrack sampling is 275 m for all cameras. In practice, most data are acquired in Global Mode, where pixel averaging is performed in order to reduce the data rate. Here 24 of the 36 data channels have been 4x4 pixel averaged before transmission from the instrument. For these channels data are transmitted at 1.1 km resolution. Even in Global Mode, however, high resolution pixels are maintained for the four nadir channels, and the eight additional Band 3/ Red channels. Complete high resolution data sets for all 36 channels can be obtained from an instrument configuration called Local Mode. Here specific sites are targeted, such as those where intensive field campaigns are being conducted. The size of a Local Mode region is 300 km downtrack by 380 km crosstrack. About a dozen Local Mode sites are acquired routinely, including observations over desert calibration sites.

## II. THE CALIBRATION PROCESS

### 2.1 On-board calibrator

Radiometric data products include geo-located radiance images at nadir and off-nadir Earth view angles. These are band-weighted camera-incident radiances, in units of  $\text{W m}^{-2} \text{sr}^{-1} \mu\text{m}^{-1}$ . The MISR radiometric response scale is established by use of an on-board calibrator (OBC), as well as vicarious calibration experiments (Bruegge et al. 1993). The strength of the OBC is its ability to provide camera, band, and pixel-relative calibrations. Experiments using the OBC are conducted once every two months. The bi-monthly frequency is desirable in that it is prudent to deploy the calibration panels only as needed to capture camera response

changes. (The MISR cameras are degrading by no more than 2% per year, as reported by Bruegge et al. 2002.) The OBC consists of two Spectralon diffuse panels, and six sets of photodiode detectors. The latter measure solar-reflected light from the panels, and provide a measure of the camera-incident radiance. These are regressed against the camera output, in order to provide the radiometric response for each of the 1504 CCD detector elements per line array, nine cameras, and four spectral bands per camera.

Although OBC system degradation can be taken into account, experiment accuracy has been increased due to the stability of the calibrator with time. Pre-launch testing (Bruegge et al. 1993, Stiegman et al. 1993) established Spectralon preparation and handling procedures which would reduce the risk of on-orbit degradation. Hydrocarbon contaminants introduced during manufacture or testing, such that due to machining oils, were shown to cause degradation once exposed to on-orbit vacuum ultraviolet light. With this information at hand the MISR Spectralon panels were vacuum baked, following laboratory reflectance testing, to remove any such contaminants. In addition, the project elected to swap out the panels present during instrument integration and spacecraft-level testing. Prior to launch the original panels were removed and replaced with panels that had been kept in a nitrogen purged container. Degradation analysis (Chrien et al. 2002) subsequently demonstrated the success of this plan. The flight Spectralon panels have degraded, on-orbit, by no more than a total of 0.5%.

Not all of the monitoring photodiodes have remained stable on-orbit. The blue High Quantum Efficient (HQE) device, a light-trapped 3 detector radiometer, has remained stable to better than 0.5% throughout the mission. This diode is therefore used as the primary standard - all other photodiodes are re-calibrated against this standard prior to the bi-monthly data analysis.

The reduction of the OBC experiment data begins with an assumption that the instrument response can be modeled as:

$$\text{DN} - \text{DN}_0 = G_1 L_b \quad (1)$$

where:

- $L_b$  is the spectral incident radiance, weighted over the sensor total-band spectral response function,
- DN is the camera output digital number,
- $\text{DN}_0$  is the DN offset, unique for each line of data, as determined by an average over the first eight "overclock" pixel elements (output samples which follow clocking of the CCD line array), and

- $G_1$  are response coefficients which provide the radiometric calibration of a specific pixel.

Originally it was believed that the photodiodes could be used to measure panel-reflected light as the Sun-panel path traversed through a varying amount of the Earth's atmosphere. This would provide radiance and DN points along the sensors response curve, including low-light levels, and hence determine camera linearity and offset. This procedure was eventually eliminated in favor of a two point calibration. The present methodology makes use of DN and radiance pairs measured when the Sun-spacecraft path is free of the Earth's atmosphere. As the dark current is too small to measure, the DN value assumed for a zero incident radiance is equal to the system electronic bias, as measured by  $DN_0$ . Several lines of evidence have led us to the conclusion that we should not include the atmospherically attenuated data. These are:

1) Photodiode linearity. The linearity of the photodiodes cannot be validated at light levels less than  $\rho_{toa}$  less than 0.03. Levels below this are outside the linearity range of their preamplifiers.

2) Photodiode offset. A finite photodiode output offset is known to exist, but not well characterized, due to digitization error for these units. Offset knowledge would be required for low-light measurements, but can be ignored in the present two point calibration.

3) Refraction effects. Refractive effects as light traverses the Earth's atmosphere further complicate the utilization of low-light levels during the bi-monthly experiments. Refraction would be spectrally dependent, resulting in a signal that varies in time by both intensity and spectral content.

4) Bi-directional reflectance factor (BRF) uncertainties. There is increased uncertainty in the laboratory measured BRF database for large illumination and view angles, as are encountered at low-light levels. For these cases Spectralon becomes non-lambertian and the BRF increases. It is feared that in this region of rapidly changing BRF is a higher uncertainty in the value. For this reason it has been decided that the OBC data process will not use data in which the sensor view angle is outside the limits of the measured BRF database.

These issues have led the MISR team to prefer a linear calibration equation to more complex forms.

## 2.2 Process updates

MISR radiometric coefficients are delivered in a file named the Ancillary Radiometric Product (ARP). Over time the processing algorithm used to derive these coefficients has changed. Table 2 summarizes these revisions. Each change has resulted in an incremental reduction in the uncertainties of the resulting radiometric coefficients. From this table we see that a band adjustment was made to MISR radiances,

Table 2. Ancillary Radiometric Product algorithm revision history

### Band-adjust.

- Decreases Red band radiance by 3% and NIR by 1%
- Impact: Radiances are more consistent with vicarious
- Date: T24\_1: Nov. 24, 2003

### Linear equation & off-axis correction (linear-offset).

- A linear calibration is restored.
- Data ignored that are contaminated by the Earth's atmosphere.
- Fixes error in BRF indexing code.
- Impact: - Linear equation is less risky.
- Eliminating data contaminated by the Earth's atmosphere increases experiment accuracy.
- Error fix does not impact on-axis radiances.. Greatest improvement is for An west edge of swath (10% change).
- Date: T17\_1: Oct. 21, 2002

### Provisional.

- The South Pole calibration panel is shown to have measured bi-directional reflectance function (BRF) data which agree with the preflight determination. The goniometer is used to update the BRF profile for the North calibration panel.
- Impact: Aft-camera radiances decreased by a few percent.
- Date: T12\_1: Dec. 22, 2001

### Quadratic.

- A quadratic calibration equation is introduced, believed to show an improvement in the radiances reported over dark targets, such as oceans.
- Impact: Changes in MISR reported radiances are negligible for equivalent reflectances  $>0.02$ , and a few percent otherwise.
- Date: T8\_1: May 17, 2001

### VC scaling.

- The June 11, 2000 vicarious calibration experiment is used to calibrate the HQE-Blue photodiode standard.
- Impact: 9% increase in MISR radiometric scale resulting from calibration of flight photodiode standard.
- Date: T2\_5: Feb. 15, 2001

### HQE-Blue.

- The blue-filtered HQE photodiode is used as the primary radiometric standard. This device is selected based upon its stability with time.
- Impact: First calibration attempt. Uses preflight calibration of the Blue HQE diode - on-orbit validation not yet in place.
- Date: T2\_4: Aug. 24, 2000

beginning with data processed after November 2003. The analysis that led to this adjustment is given in Section 2.4, and is based upon studies of data processed with the previous, or "linear-offaxis" processing algorithm.

In order to understand the data heritage, MISR investigators should document the ARP version used to generate their data. To determine which ARP file was used to produce a Level 1B1 data product, one would use an HDF browser, such as hdfscan. (This software is available from the Langley DAAC, <http://eosweb.larc.nasa.gov>, and was written to view MISR data as well as generic HDF files). Using such a data browser, one can read the metadata published within the MISR data product. The ARP file name can be found under Annotation Text: Input Data files. This file name can be compared to the latest delivered ARP file name, for a specific time period.

### 2.3 Vicarious calibration

MISR has conducted annual vicarious field campaigns, using desert targets in Southwestern United States. As MISR radiances change with processing algorithm updates, the ratio of MISR to VC radiances may also change. In order to look for consistent biases with respect to MISR, a comparison must be made with a common processing algorithm. This was done using the "linear-offset" algorithm, that was in place through October 2003. The results are shown in Figure 1.

-----  
Figure 1. AN camera vicarious calibration results - Nadir Terra overpass dates.

For these experiments data were acquired at Lunar Lake (LL), Railroad Valley (RRV), Ivanpah (Ivan), and Black Rock Desert (BRD). Of these Ivanpah is the smallest in extent, roughly a km across. These data are exceptionally low, indicating that some residual out-of-field effect may still be present, at the 1% level. (MISR Level 1B data are corrected for point-spread-function response, as part of the standard processing). Excluding these data, the precision of the vicarious calibration process appears to be in the 2-4% level - smallest for the Green and Red spectral bands. The mean of these calibration is shown with "dot" symbols as a line indicator. These data indicate that there is no systematic change in the reported MISR calibration, to within the precision of the vicarious calibration methodology. For this reason, no updates have been made to the response coefficient of the OBC primary photodiode standard, other than its initial adjustment in February 2001.

### 2.4 Band-relative adjustment

Inspection of Figure 1 suggests that the MISR Red and NIR bands are biased high, with respect to vicarious calibration results. For these "linear-offset" data, the band-relative scale is determined as follows:

1) The June 2000 VC campaign is used to calibrate the OBC primary standard, the HQE-Blue photodiode. If needed future VC experiments could be used to update the response of this primary standard.

2) For each bi-monthly experiment the measured radiance from the Blue-HQE photodiode is used to predict the band-weighted radiances for the other photodiodes. Differences in field-of-view are taken into account, and the Spectralon reflectance is assumed to be spectrally invariant.

3) The response coefficient of each of the secondary diodes is adjusted such that the measured and predicted radiances agree. This step removed any response degradation from the secondary photodiodes.

4) The secondary photodiodes are used to calibrate each camera: Blue PIN photodiodes used to calibrate Blue-filtered cameras, and similarly for the other spectral bands. The nadir-viewing PIN are used to calibrate the An camera; the off-nadir PIN is used to calibrate the off-nadir cameras. (A PIN photodiode is constructed with a single diode per packaged, hence a simpler configuration than the HQE light-trapped design.)

Figure 1 suggests that there is an inconsistency with wavelength, in comparing VC radiances to MISR-measured radiances. In particular, looking at the mean VC comparison, we see that the MISR radiances are 3% too high in the Red, and 1% too high in the NIR.

Figure 2 shows this same mean VC result, but in addition plots the MISR-Lunar comparison, to be discussed in Section 4.2. For the Lunar curve a 5% bias was removed at all wavelengths. (A band-relative only comparison is required here.) The consistency of these band-relative results is striking, and demonstrate that findings are consistent over a range of target radiances and scene contrasts. The desert targets are roughly 0.3 in equivalent reflectance, the lunar surface approximately 0.04; the desert target is homogeneous and extensive, while the lunar target covers only a fraction of the MISR field-of-view.

This comparison validates the postulate that MISR has too high a response, in the Red and NIR. As a result of this study, the MISR radiance products will be decreased by 3% in the Red and 1% in the NIR. This change is effective for all data processed after November 2003.

Figure 2. Comparison of mean vicarious calibration results with bias-removed Lunar data.

In order to investigate why the OBC band-relative scale differs from the VC scale, we reviewed the assumption that Spectral is spectrally neutral across our bandpasses. Early et al. (2000) published results of a BRF-measurement which involved several institutions, including JPL and National Institute of Standards and Technology (NIST). From this study we see that reflectance of Spectralon is 0.1% larger than that assumed for our BRF database, the latter being based upon HeNe laser data acquired at 632 nm. This result is for a solar illumination angle of 45° and for the nadir viewing pixels. Although the Early report does suggest there is some wavelength dependence to the Spectralon's reflectance, we do not believe it is sufficient to explain the 3% adjustment required for our Red band. Unfortunately, the correction must compensate for a systematic error of unknown origin.

### III. ERROR-TREE ANALYSIS

#### 3.1 Electronic offset: Baseline stabilization

MISR camera signal chains incorporate a circuitry called BaseLine Stabilization (BLS). The BLS circuitry was incorporated into the MISR design in order to adjust for sudden changes in the system response, as could follow radiation-induced damage to the detector, or in the event of undesirable operational amplifier feedback. The circuitry adds a floating electronic pedestal to the signal chain. In the presence of a sudden change in the incident illumination, the BLS stabilizes its output in about 75 lines (3 seconds). In order to measure the light-induced portion of the signal, this offset must be subtracted. We estimate this offset by use of overclock pixels. The MISR clocks out 512 samples of the serial register, following reading of the light-sensitive portion of the signal chain. Of these, eight are transmitted with the active-pixel data. An average of these overclock pixels is computed, and used as a measure of the electronic offset,  $DN_0$ . The BLS circuitry also makes use of these overclock pixels to drive the signal chain electronics to -2.9 V, when no optical illumination is present. It is not known whether the BLS circuitry samples the same samples that are transmitted to the ground.

There are several uncertainties associated with usage of the BLS circuitry:

- Preflight testing has showed that the 512 overclock pixels are not constant for a given line of data. Further,

we do not know which of the 8 overclock samples are used to establish the BLS output which controls the magnitude of the electronic offset. There is therefore some uncertainty, which can be quantified as the difference in the overclock over the 512 samples.

- In theory the BLS should be independent of illumination level. This is found not to be the case, presumably because of light leaking into the serial register even when the CCD signal has been clocked out. This deviation reduces our confidence in measuring the electronic offset. A light leak would cause  $DN_0$  to underestimate the electronic bias signal.

- The effective offset signal could vary spatially across the active array, and thus no one value of  $DN_0$  would accurately represent the electronic bias. Light leakage into the serial array is one such mechanism by which a spatially variable bias signal could be induced across the CCD array.

With these potential errors we wish to bound the radiometric uncertainty due to BLS. If we are correctly using the first 8 overclock samples as a correct representation of the electronic pedestal, then there is no error in the static-illumination case. If instead the electronic pedestal is best represented by the latter overclock samples, then the error is 21 counts out of 300 DN. This is a 7% error for the 2% equivalent reflectance signal. This uncertainty error due to BLS would be larger for mixed ocean/ cloud or ocean/ snow and ice scenes. Here the bright targets would drive up the overclock as well as contribute to leakage into the shield register.

-----  
Figure 3. Extended overclock pixels as measured during preflight testing. Each line is the response to integrating sphere illumination, spanning the range of equivalent reflectance from 0.05 to 1.0.

#### 3.2 Electronic offset: Dark current

Full well is roughly a million electrons over our 14-bit system. Thus, we have about 60 e- per DN bin. The CCD readout rate is 40 msec, and that the pixel size is 21  $\mu\text{m}$ . The dark current can be expressed as:

$$D = 2.5 \times 10^{15} P N T^{1.5} e^{-E_g/(2kT)} \quad (2)$$

where P is the pixel size ( $\text{cm}^2$ ), N is the dark current at 300K, 26.85 C ( $\text{nA}/\text{cm}^2$ ),  $E_g$  is the silicon band-gap energy (eV), and T the operating temperature (K). (This equation has come from Janesick, Thermal dark current tutorial, <http://www.pvinc.com/janesicks-therm-letter.htm>).

This equation shows that for our -5 C operating temperature, the Dark current is 1 DN. It is noted that this is an overestimation, as charge is collected only over the integration time (roughly 20 msec), and that the actual pixel area is 21x18  $\mu\text{m}$ .

In reviewing MISR's measured dark current, we have observed a dark current of 0 or 1, for both preflight and on-orbit conditions. Thus, this theoretical prediction agrees with the calculations given here. We conclude that dark current is not inducing a reduction in radiometric accuracy, even for dark targets.

### 3.3 Signal chain: Square-root encoding

MISR makes use of square-root data encoding, in order to decrease the data rate required from the spacecraft to the ground station. The algorithm to encode MISR digital numbers (DN) into a compressed number is as follows:

$$\text{DN\_encoded} = \text{round}(32.0 * \text{sqrt}(\text{fbat}(\text{DN}))) \quad (3)$$

During data processing at ASDC these numbers are restored to their linear representation. To decode these numbers, the following operation is performed:

$$\text{DN\_L1A} = \text{round}(\text{fbat}(\text{DN\_encoded}) / 32.0^2) \quad (4)$$

One can now estimate the percentage radiometric error, by assuming a typical overclock value:

$$\text{DN\_overclock} = 350 \quad (5)$$

$$(6)$$

$$\% \text{\_error} = (\text{DN\_L1A} - \text{DN}) * 100. / (\text{DN} - \text{DN\_overclock})$$

It is thus shown that the radiometric error attributable to square-root encoding is 0.5% for DN greater than 200 DN above overclock (an equivalent reflectance of 0.005), and decreases with increasing illumination. The error due to square-root-encoding is therefore considered negligible.

### 3.4 Optical effects: Ghosting

Figure 4 shows an iceberg surrounded by a dark ocean. The image was acquired on December 9, 2001, over the Ross Sea. The lower image shows a highly contrast-stretched image of the normal view, shown above. The iceberg shown in the lower figure is an inverted, blurred ghost image of the original iceberg. The reflectance of the ice is approximately 0.4, all bands, whereas the ocean reflectance varies from 0.06 to 0.01 in going from the Blue to NIR wavelengths. In this image 0.3% of the bright target has been reflected into the adjacent dark ocean. For ghosting of this magnitude, a target brighter than  $\rho_{\text{toa}} = 0.66$  would be required in order to induce a radiometric error of 10% in a dark ocean scene of

magnitude 0.02. The dark target would have to be located specifically in the ghost location. We conclude that for all but a small number of cases, ghosting will not impact radiometry over dark ocean targets.

-----  
Figure 4. Ghosting in the MISR Bf-NIR band. Data were acquired over the Ross Sea, Orbit 10521, Path 54. The ice TOA reflectance is on the order of 0.43, with a dark ocean of 0.06 - 0.01 for the Blue to NIR bands.

It is difficult to correct for the ghosting, as the secondary image is not in focus. Any attempt to remove the ghost has resulted in a shadow where the image had been. We also know that only the A and D cameras were tuned to produce blurred ghost images. This was never done for the B and C cameras. The degree of focus for these images, therefore, is camera dependent.

### 3.5 Optical effects: Point-spread-function response

The image of a point object source is always blurred due to diffraction, lens aberrations, and scattering. The output response to a point source is known as the point-spread-function (PSF) for a given optical system. MISR PSF functions have been measured pre-flight.

As an in-flight validation of the PSF, the derivative of the edge response was taken, using the iceberg edge of the December 9, 2001 Antarctica scene. The updated response was found to have the same shape, but with a larger halo, as compared to the preflight measurement. These preflight and in-flight derived PSF kernels are shown in Figure 5. This figure indicates that the preflight PSF's underestimate the amount of contrast adjustment needed.

-----  
Figure 5. Comparison of preflight and inflight empirical PSF's.

PSF correction is done on all MISR radiance data products. The operational PSF functions were derived by the following procedure:

- 1) Start with the preflight point spread function
- 2) Average right and left about the center to make it symmetric.
- 3) Multiply the entire function by a scale factor which adjusts the background halo to that empirically derived from the on-orbit data.
- 4) Renormalize to unit area by adjusting the energy in the central 3 pixels (which contain ~95% of the energy)

- 5) Take 1/Fourier transform. If this function were inverse transformed, it would result in a deconvolution kernel that would induce ringing
- 6) Prior to inverse FT, multiply 1/Fourier transform by the Fourier transform of the central 9 pixels of the PSF (the "core").
- 7) Inverse transform, take the real part, and average left/right to correct any numerically-induced asymmetries

A value of 1.5 has been used to produce the operational kernels. It is believed that this procedure minimizes the ringing associated with a sharper PSF core, and improves the contrast.

It is believed that radiometry is not impaired due to uncorrected PSF effects, for locations at a distance greater than eight pixels from a contrast edge. This has been validated by inspection of iceberg edges.

#### IV. CROSS-COMPARISON STUDIES

##### 4.1 MODIS

MODIS is an ideal sensor with which to cross-compare radiometric products. The MODIS passband parameters, when derived using the MISR moments analysis algorithm, are listed in Table 2. The MODIS land Band 4 and ocean Band 9 are examples of bands that are well matched for the two sensors. For all bands a radiometric correction is made to predict the radiance that MODIS would have reported, had it been built with MISR band-passes. The spectral algorithm has been described in Bruegge et al. (2002). Comparisons reported in this Section have all had these spectral corrections performed.

MODIS reports a reflective solar bands (RSB) calibration uncertainty of 2% for the reflectance factor and 5% for the radiance product. Both land and ocean

channel calibrations utilize a solar diffuser (SD). In addition to a direct view of the panel, a second data set is acquired using a 7.8% transmission screen deployed in front of the SD. This calibrates those channels that would otherwise saturate.

The MODIS detectors view the calibrated SD to place their data products on a top-of-atmosphere (TOA) reflectance scale. The measurement precision is about 0.2 to 0.5% depending on the bands or if the SD screen is used in the calibration (ocean bands use SD screen for the calibration). SWIR band uncertainties are higher due to residual crosstalk errors.

The solar diffuser stability monitor (SDSM) is used to track SD degradation. The SDSM is a small integrating sphere and filtered detectors which look at the sun and SD respectively. The ratio of the SD to the sun view provides a measure of the spectral reflectance of the SD, thus tracks the SD degradation. The SDSM makes use of a 2% transmission screen when viewing the Sun. This is done to place the incoming signal on the same point on its dynamic range curve.

More recent data uses a direct view of the SD for both the land and ocean channels. The difference in using the screen or not using the screen is less than 1%. Thus we believe the relative calibration between the ocean and land bands is within 1%.

Figure 6 below compares the radiances measured by several sensors against the vicarious calibration radiances. For comparisons over uniform desert playa, MISR is typically 3-7% brighter when using MISR data of "linear-offaxis" heritage. The agreement is therefore within 4% for MISR band-adjusted data. The radiometric bias between MISR and MODIS can be traced to the utilization of different standards and processes used to establish their respective scales. (Kurt

Table 2. MODIS spectral parameters

| MISR<br>Band no. | Sensor        | $\lambda_c$ , nm | $\delta\lambda$ , nm | $E_{0,b}$ [ $\text{W m}^{-2} \mu\text{m}^{-1}$ ] | Sensor/ MISR radiance<br>scale factor |       |
|------------------|---------------|------------------|----------------------|--|---------------------------------------|-------|
|                  |               |                  |                      |  | Desert                                | Ocean |
| 1                | MODIS Band 3  | 466              | 21                   | 2015   | 0.906                                 | 1.054 |
| 2                | MODIS Band 4  | 554              | 21                   | 1858   | 1.002                                 | 0.978 |
| 3                | MODIS Band 1  | 646              | 50                   | 1601   | 0.986                                 | 0.903 |
| 4                | MODIS Band 2  | 856              | 45                   | 989.8  | 0.982                                 | 0.997 |
| 1                | MODIS Band 9  | 442              | 11                   | 1865   | 1.010                                 | 0.978 |
| 2                | MODIS Band 12 | 547              | 12                   | 1870   | 1.012                                 | 0.933 |
| 3                | MODIS Band 14 | 677              | 14                   | 1505   | 1.003                                 | 1.027 |
| 4                | MODIS Band 16 | 866              | 19                   | 969.7  | 1.005                                 | 1.029 |

Thome, University of Arizona, provides VC datasets for the MODIS team, and reports a discrepancy of -1.4, -0.9, -3.4, -2.5, and -3.4% respectively, for the MODIS 412, 469, 555, 645, 858 nm bands. MODIS radiances are lower than his VC observations.) MODIS VC studies are done using their land channels, as the ocean channels saturate over these bright targets.

-----  
Figure 6. Measured radiances from Vicarious Calibration data, MISR, MERIS, MODIS, and Landsat. Data were acquired July 22, 2003 at Railroad Valley, Nevada.

MISR and MODIS comparisons were next made over uniform dark oceans. One such example is provided in Figure 7. Here the MISR and MODIS ocean radiances show the same spectral shape, with MISR again reporting larger radiances. It is noted that the MODIS land channels, particularly Band 3, seem to be discrepant as compared to the other measurements. It is therefore noted that MISR and MODIS agree reasonably well, but with a finite bias, when MODIS land bands are used to view land scenes, and when MODIS ocean bands are used to view ocean scenes.

-----  
Figure 7. A comparison of radiometry from MISR, MODIS land channels, and MODIS ocean channels, for a dark ocean target.

One final figure, Figure 8, shows the ratio of MISR and MODIS land channels for a scene that is predominantly land (right half of image), and predominantly ocean (left half of image). It is noted that the ratio increases over ocean. This suggests a non-linearity in one or more sensors. It is noted that MISR is an all refractive system, with a Lyon depolarizer as its front element. MISR is insensitive to polarization effects. This may be one explanation of the differences for this scene. A more detailed validation of MODIS radiometry, using the ocean bands, is on-going by the MODIS ocean community. Further validation studies on the radiometric response of MODIS land channels, over dark ocean targets, is needed. (It is noted that MODIS land channels are used to retrieve aerosol properties over ocean sites.)

-----  
Figure 8. Top) Plot of mean equivalent reflectance across the Arabian Sea image shown in previous figure. The mean is calculated by averaging MISR radiances in the vertical (north-south) direction. Standard deviations around the mean are also shown. High standard deviations are where both land and water figure into the calculations. Bottom) Median MISR/ MODIS radiance ratio at each sample location, calculated by combining all

points in the north-south direction. Standard deviations are also shown. Note the inconsistency between the ratio over water (dark scene) relative to land (bright scene).

#### 4.2 Lunar observations

Lunar observations are routinely used by SeaWiFS (Barnes et al. 1999), an ocean viewing sensor, to track degradation with time. On April 14, 2003, MISR had its first opportunity to view the moon. A special maneuver of the Terra spacecraft was performed, on this date, as it traversed the nightside of the orbit. The maneuver entailed a backwards somersault of the spacecraft as it pitched end-over-end, allowing the normally Earth-viewing instruments to look at deep space and the waxing gibbous Moon. The purpose of this acrobatic feat was to assist in the cross-comparison of MISR, MODIS, and ASTER (all Terra instruments) as well several other sensors on an assortment of platforms. During a 16-minute interval, the lunar disk passed through the fields-of-view of all nine MISR cameras, resulting in a unique set of images. Figure 9 shows one such image, for the high-resolution Df-Red channel. Familiar lunar features are clearly recognizable. The dark lunar "maria" are vast plains of basaltic lava.

-----  
Figure 9. High resolution Lunar image, Df\_Red channel.

Lunar data were acquired in Global Mode, with 12 high-resolution channels (Fig. 10a) and 24 channels in 4 pixel by 4 line averaging mode, called 4x4 (Fig. 10b). Varying resolution is also encountered with the four camera designs, due to differences in focal lengths. Examples of the resolution with camera design are shown in Figure 11.

-----  
Figure 10. MISR viewed the moon in its baseline Global Mode configuration. Here twelve of the 36 MISR channels are configured to high-resolution (no averaging) during Global Mode, as shown in (a). Twenty four channels are in 4x4 pixel averaging mode, (b).

-----  
Figure 11. Lunar image resolution degrades in going from the D to A camera design, due to the smaller focal lengths in going from D to A..

These data were then used to derive a measure of the Lunar irradiance, which was compared to that of the empirically derived Robotic Lunar Observatory (ROLO) model. In computing this irradiance, we must account for a large amount of oversampling. The equation used for this analysis sums the radiance

samples, multiplies by the detector solid angle, and corrects for oversampling.

(7)

$$\begin{aligned} \text{Lunar Irradiance } [\mu\text{W m}^{-2} \text{ nm}^{-1}] = & \\ & (\text{fraction of IFOV not in previous samples}) * \\ & (\text{detector solid angle [sr]}) * \\ & (\sum L [\mu\text{W m}^{-2} \text{ sr}^{-1} \text{ nm}^{-1}]) \end{aligned}$$

The required inputs are given in Table 2.

Table 2. Lunar calibration parameters for April 14, 2003

---

|  |
|--|
| Lunar observation date: April 14, 2003   |
| Orbit: 17672   |
| Time: 2200-2220 UT   |
| $\Delta$ [rad/ sec]= 0.002129, the planned Terra pitch rate 0.122 deg/ sec                       |
| D [1000 km] = 366.5-6371/ 1000-1738/1000-0.705=357.7   |
| $t_{\text{samp}}$ [msec] = 40.8, MISR camera sampling rate                                       |
| f [mm]={123.67, 95.34, 73.02, 58.90, 58.90, 59.03, 73.00, 95.32, 123.65} for Df-Da camera        |
| $\Delta x_{\text{det}}$ [ $\mu\text{m}$ ] = 21, crosstrack detector dimension                    |
| $\Delta y_{\text{det}}$ [ $\mu\text{m}$ ] = 18, alongtrack detector dimension                    |
| $\sum L$ [ $\mu\text{W m}^{-2} \text{ sr}^{-1} \text{ nm}^{-1}$ ], sum of MISR radiance samples  |
| fraction of IFOV not in previous sample = $t_{\text{samp}} * \Delta * f / \Delta x_{\text{det}}$ |
| detector solid angle [sr] = $\Delta x_{\text{det}} * \Delta y_{\text{det}} * 10^{-6} / f^2$      |

---

The results of this comparison is shown in Figure 12. Although there appears to be a 5% bias between MISR and ROLO, in fact a similar bias is found between the ROLO model and SeaWiFS, as well as between the model and MODIS ocean channels (Kieffer 2003). It is concluded that the Lunar observations confirm that MISR radiometry is consistent with MODIS ocean channel, as well as SeaWiFS, for this low-light target.

The accuracy of the MISR measure of radiance is limited by the oversampling correction. It is believed to be uncertain to at least 5%, based upon the scatter of measurements from the nine MISR cameras. Nevertheless, the experiment proved to be extremely valuable for the MISR community, in that it validated the band-adjustment values obtained from the vicarious calibration experiments, as well as confirmed that the absolute radiometry is consistent with comparisons made over land targets. Our confidence in MISR radiometry over low-level targets is therefore increased due to this experiment.

-----  
Figure 12. Differences between MISR, MODIS, and SeaWiFS, as compared to the ROLO measure of lunar irradiance.

## V. CONCLUSIONS

The MISR calibration and science teams have carefully reviewed the contributors to radiometric accuracy over low-light scenes. As with any instrument, radiometry for these conditions is challenging. We have investigated the impact of electronic bias, dark current, and data compression, and find that these error terms do not degrade the quality of the data. Further, cross-comparison with MODIS over both ocean and lunar observations demonstrate the consistency of these data. For these reasons we believe that MISR is meeting its absolute calibration specification for dark water conditions, including an uncertainty specification of 10% at  $\rho_{\text{toa}}=0.02$ . Further, for data processed after November 2003, we believe that the band-relative requirement for an uncertainty of 1% is also being met throughout the dynamic range of the instrument.

Linearity not properly measured, effects of BLS uncertain. Cross-comparison and dark water VC experiments best way to validate radiometry over dark water targets.

30% of late  
30% of late  
30% of late

## VI. ACKNOWLEDGMENTS

The work described in this paper is being carried out at the Jet Propulsion Laboratory, California Institute of Technology, under contract with the National Aeronautics and Space Administration. MISR data products are processed and made available by the The Atmospheric Sciences Data Center, Langley Research Center.

A number of support individuals have assisted in the acquisition and analysis of MISR calibration data, including Mike Smyth, David Nelson, Kyle Miller, Tom Thaller, and Tom Nolan. The authors also wish to thank the following individuals who have participated in Peer Reviews of MISR calibration: Roger Davies, Michael Gunson and Cinzia Zufada, JPL; Brian Markham, Landsat Calibration, GSFC; Stu Biggar, Vicarious calibration, Univ. of Arizona; James Butler, EOS Calibration Scientist, GSFC; Bruce Guenther, MODIS Calibration, GSFC; and Jeff Mendenhall, ALI Design Engineer, Lincoln Labs.

Finally, Jack Xiong, GSFC is to be thanked for many hours spent reviewing the MISR versus MODIS comparisons.

## VII. REFERENCES

- Abdou, W., C. Bruegge, M. Helmlinger, J. Conel, S. Pilorz, & B. Gaitley 2002. *Vicarious calibration experiment in support of the Multi-angle Imaging SpectroRadiometer (MISR)*, IEEE Trans. Geosci. Remote Sens., 40(7): 1500-1511.

Barnes, Robert A., Robert E. Eplee, Jr., Frederick S. Patt, & Charles R. McClain 1999. *Applied Optics* 8(21):4649-4664.

Bruegge, Carol J., Nadine L. Chrien, Robert R. Ando, David J. Diner, Wedad A. Abdou, Mark C. Helmlinger, Stuart H. Pilorz, & Kurtis J. Thome 2002. *Early Validation of the Multi-angle Imaging SpectroRadiometer (MISR) Radiometric Scale*, IEEE Trans. Geosci. Remote Sens. 40 (7): 1477-1492.

Bruegge, C., V. Duval, N. Chrien, & D. Diner 1993. *Calibration Plans for the Multi-angle Imaging SpectroRadiometer (MISR)*, Metrologia 30(4):213-221.

Bruegge, C., A. Stiegman, R. Rainen, A. Springsteen, 1993. *Use of Spectralon as a diffuse reflectance standard for in-flight calibration of earth-orbiting sensors*, Opt. Eng. 32(4):805-814.

Chrien, N., C. Bruegge, & R. Ando, 2002. *Multi-angle Imaging SpectroRadiometer (MISR) on-board calibrator (OBC) in-flight performance studies*, IEEE Trans. Geosci. Remote Sens. 40 (7): 1493-1499.

Diner, D., J. Beckert, T. Reilly, C. Bruegge, J. Conel, R. Kahn, J. Martonchik, T. Ackerman, R. Davies, S. Gerstl, H. Gordon, J-P. Muller, R. Myneni, R. Sellers, B. Pinty, & M. Verstraete 1998. *Multi-angle Imaging SpectroRadiometer (MISR) description and experiment overview*, IEEE Trans. Geosci. Rem. Sens. 36:1072-1087.

Early, E.A., P.Y. Barnes, B.C. Johnson, J.J. Butler, C.J. Bruegge, S.F. Biggar, P.R. Spyak, M.M. Pavlov, 2000. *Bidirectional reflectance round-robin in support of the Earth Observing System program*, American Meteorological Society, August:1077-1091.

Horvath, Akos and Roger Davies, 2004.

Kahn, 2004. Dark water vicarious calibration. In preparation.

Kahn, Ralph, Pranab Banerjee, & Duncan McDonald 2001. *The sensitivity of multi-angle imaging to natural mixtures of aerosols over ocean*, J. Geophys. Res. 103(D24): 32195-32213.

Kahn, Ralph, Pranab Banerjee, Duncan McDonald, & David J. Diner 1998. *Sensitivity of multiangle imaging to aerosol optical depth and to pure-particle size distribution and composition over ocean*, J. Geophys. Res., 103(D24):32,195-32,213.

Kieffer 2003. Utah conference.

Marchand, Roger, 2004.

Stiegman, A.E., C.J. Bruegge, A.W. Springsteen, 1993. *Ultraviolet stability and contamination analysis of Spectralon diffuse reflectance material*, Opt. Eng. 32(4):799-804.

----- END -----

### VIII. UPDATES TO BE MADE

- Summarize what Ralph has to say in his publication and get citation
- Summarize Roger Marchand work and get citation
- Summarize Akos work and get citation
- Barnes, Lunar cal paper title
- What is  $\rho_{\text{toa}}$  for lunar views (average and stdev), for the 4 bands?
- redraw lunar figure (keep SeaWifs, MODIS, and MISR) & get permission from MODIS and SeaWifs
- Redraw all figures in black and white
- Reference for MODIS and its calibration system.
- Add info. from recent email on MODIS problems over dark ocean.

### IX. UNUSED REFERENCES

C. Bruegge, V. Duval, N. Chrien, R. Korechoff, B. Gaitley, and E. Hochberg, "MISR prelaunch instrument calibration and characterization results," IEEE Trans. Geosci. Rem. Sens., vol. 36, pp. 1186-1198, July, 1998.

C. Bruegge, M. White, N. Chrien, E. Villegas, and V. Ford, "Multi-angle Imaging SpectroRadiometer (MISR) design issues influenced by performance requirements," Sensor Systems for the Early Earth Observing System Platforms, Proc. SPIE 1939, pp, 104-113, April, 1993.

P. Slater, "A review of some radiometric calibration problems and methods," Proc. International Colloquium on Spectral Signatures of Objects in Remote Sensing, Bordeaux, France, 1983.

C. Bruegge, A. Stiegman, R. Rainen, A. Springsteen, "Use of Spectralon as a diffuse reflectance standard for in-flight calibration of earth-orbiting sensors," Opt. Eng. vol. 32, no. 4, pp. 805-814, 1993.

C. Jorquera, C. Bruegge, V. Duval, "Evaluation of high quantum efficiency silicon photodiodes for calibration in the 400 nm to 900 nm spectral region," Infrared Technology XVIII. Proc. SPIE vol. 1762, pp. 135-144, 1992.

D. Diner, J. Beckert, B. Bothwell, and J. Rodriguez, "Performance of the MISR instrument during its first 20 months in Earth orbit," IEEE Trans. Geosci. Remote Sens., this issue.

R. Woodhouse, C. Bruegge, B. Gaitley, G. Saghri, and N. Chrien, "Multi-angle Imaging SpectroRadiometer (MISR) Ancillary Radiometric Product (ARP)," Earth Observing System II, Proc. SPIE vol. 3117, San Diego, July, 1997.

C. Bruegge, N. Chrien, and D. Haner, "A Spectralon BRDF data base for MISR calibration applications. Remote Sens. Environment," vol. 76, pp. 354-366, 2001.

D.J. Diner, L.M. Barge, C.J. Bruegge, T.G. Chrien, J.E. Conel, M.L. Eastwood, J.D. Garcia, M.A. Hernandez, C.G. Kurzweil, W.C. Ledebauer, N.D. Pignatano, C.M. Sarture, and B.G. Smith, "The Airborne Multi-angle SpectroRadiometer (AirMISR): instrument description and first results," IEEE Trans. Geosci. Rem. Sens., Vol. 36, pp. 1339-1349, 1998.

C. Bruegge, M. Helmlinger, J. Conel, B. Gaitley, and W. Abdou, "PARABOLA III: a sphere-scanning radiometer for field determination of surface anisotropic reflectance functions," Remote Sensing Reviews, vol 19, pp. 75-94, 2000.

E. Early, P. Barnes, B. Johnson, J. Butler, C. Bruegge, S. Biggar, P. Spyak, M. Pavlov, "Bidirectional reflectance round-robin in support of the Earth Observing System program," American Meteorological Society, pp. 1077-1091, August, 2000.

World Climate Research Programme (WCRP) Publication Series No. 7, WMO ITD-No. 149, pp 119-126, October 1986. The data was compiled by Christoph Wehrli, World Radiation Center (NRC), Davos-Dorf, Switzerland under WRC Publication No. 615, July 1985.

Solar Physics, 171:283-302, 1997.

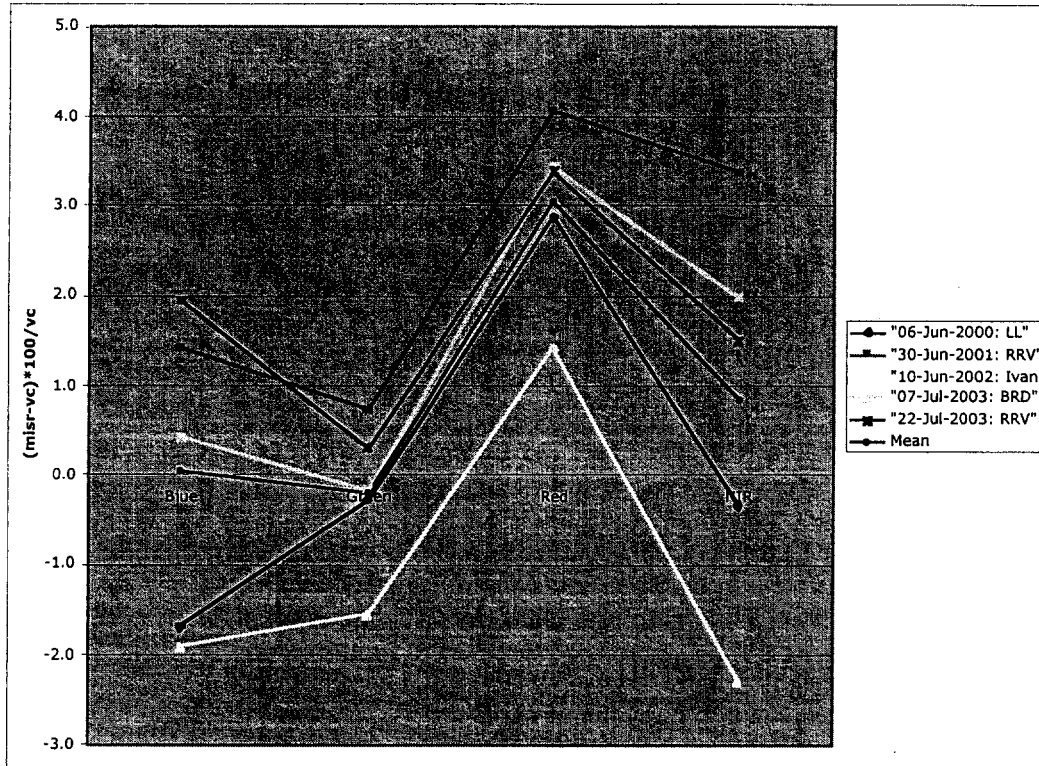


Figure 1. AN camera vicarious calibration results - Nadir Terra overpass dates.

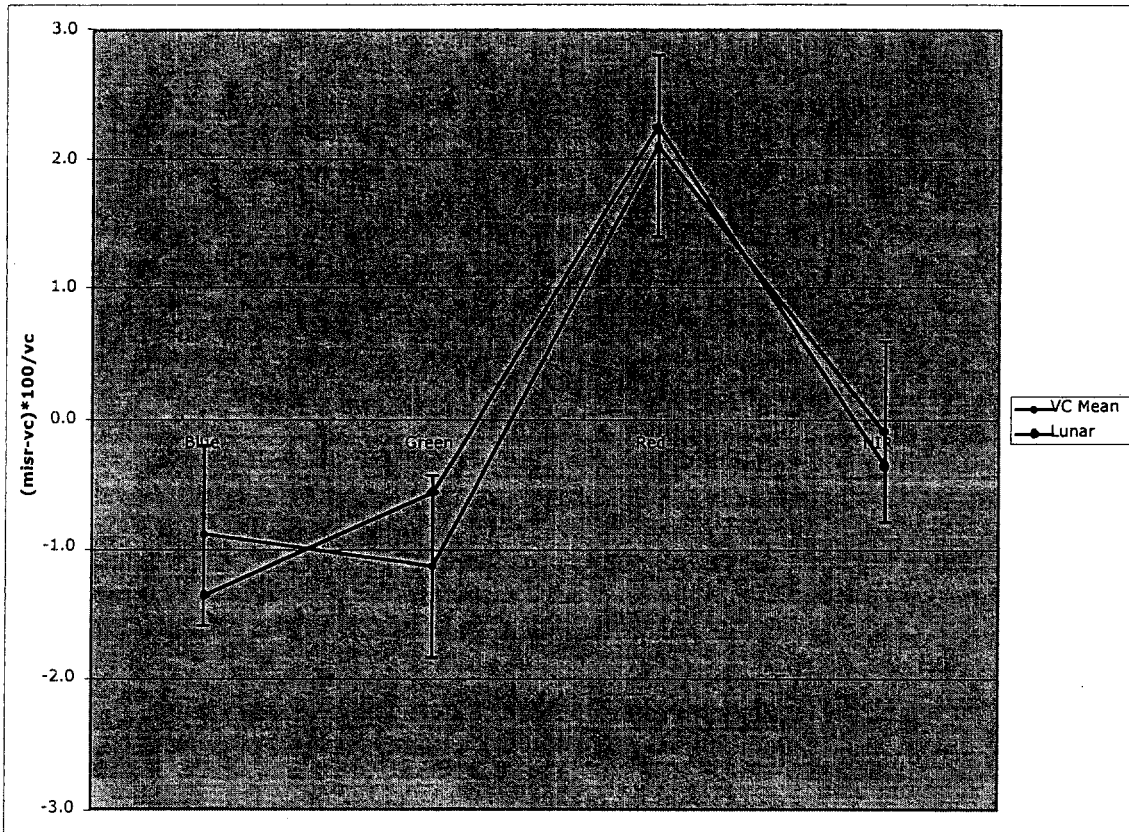


Figure 2. Comparison of mean vicarious calibration results with bias-removed Lunar data.

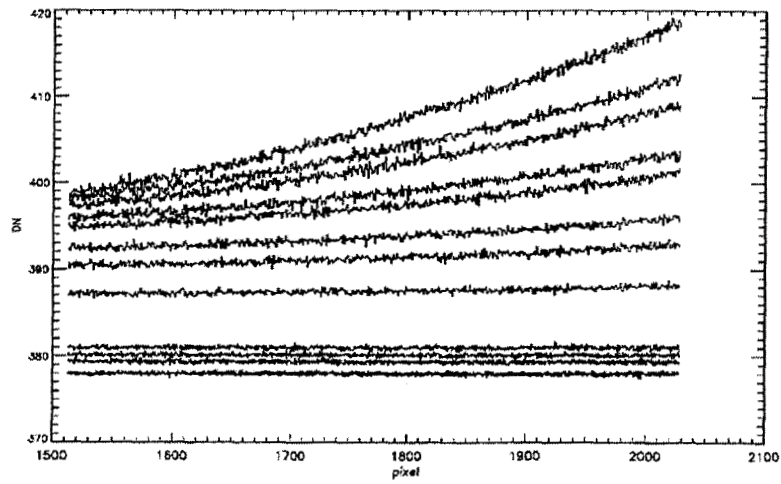


Figure 3. Extended overclock pixels as measured during preflight testing. Each line is the response to integrating sphere illumination, spanning the range of equivalent reflectance from 0.05 to 1.0.

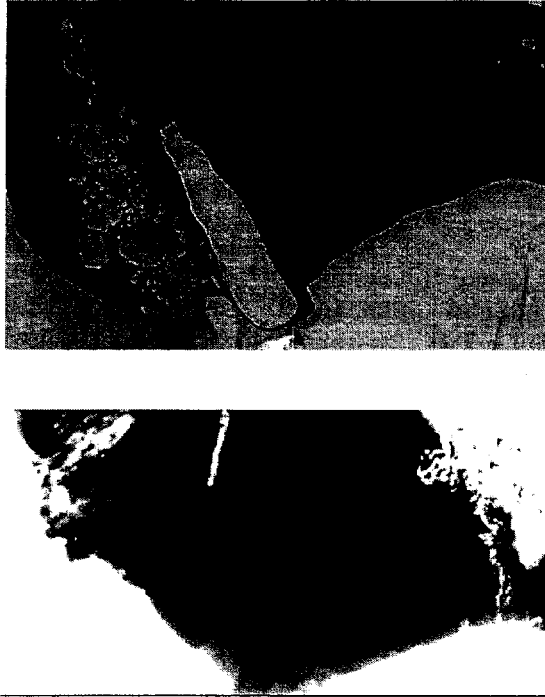


Figure 4. Ghosting in the MISR Bf-NIR band. Data were acquired over the Ross Sea, .Orbit 10521, Path 54. The ice TOA reflectance is on the order of 0.43, with a dark ocean of 0.06 - 0.01 for the Blue to NIR bands.

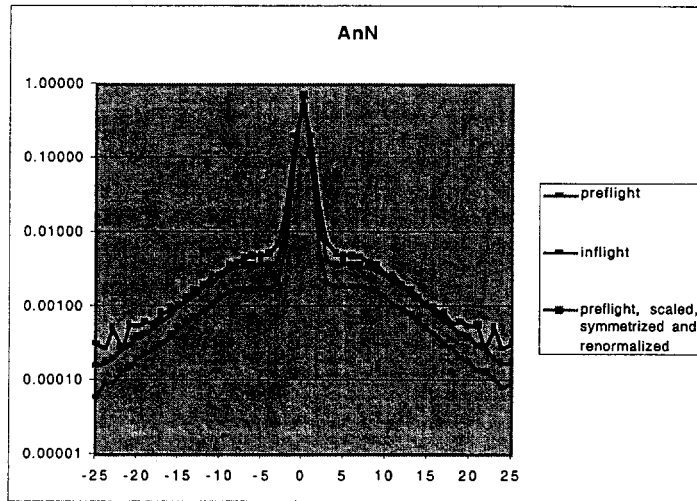


Figure 5. Comparison of preflight and inflight empirical PSF's.

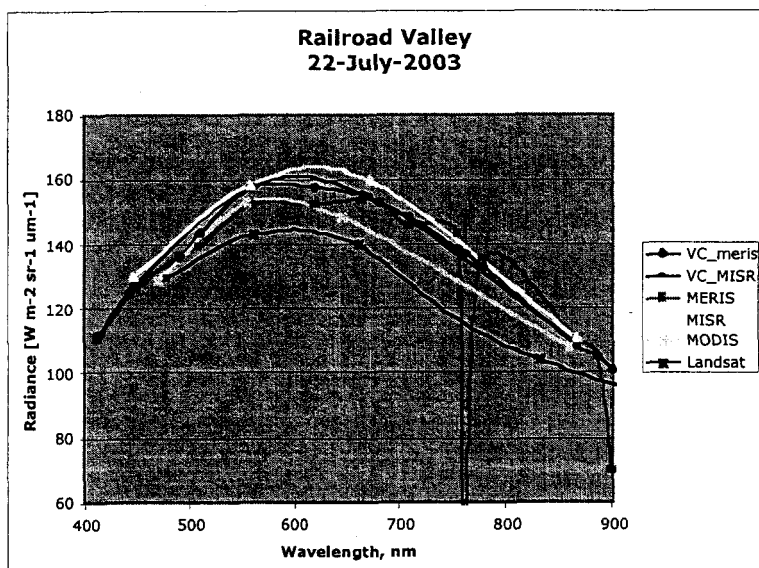


Figure 6. Measured radiances from Vicarious Calibration data, MISR, MERIS, MODIS, and Landsat. Data were acquired July 22, 2003 at Railroad Valley, Nevada.

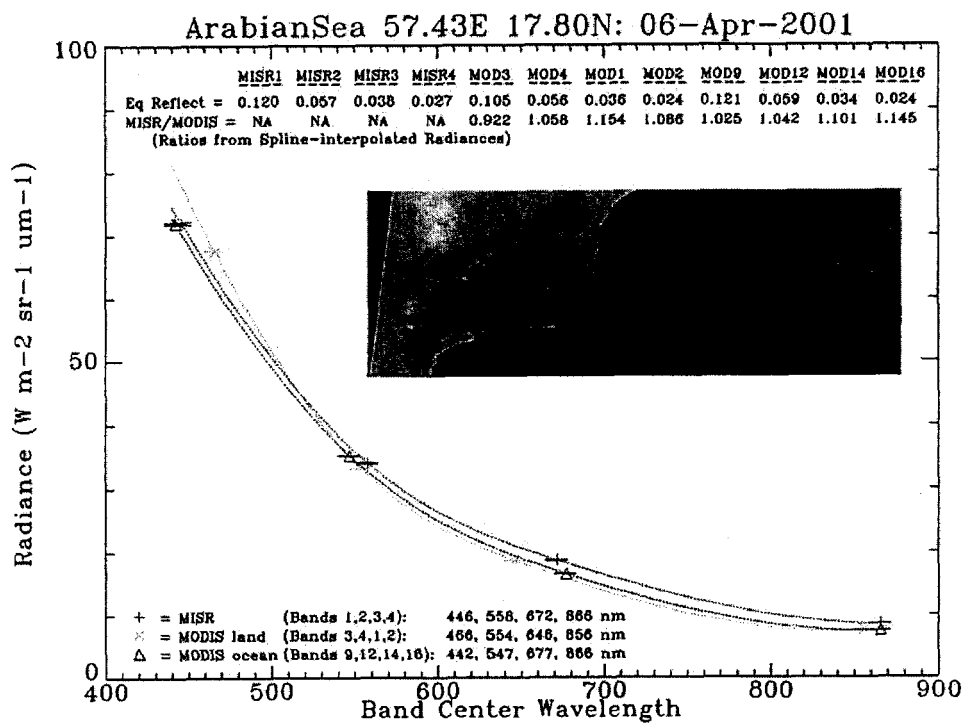


Figure 7. A comparison of radiometry from MISR, MODIS land channels, and MODIS ocean channels, for a dark ocean target.

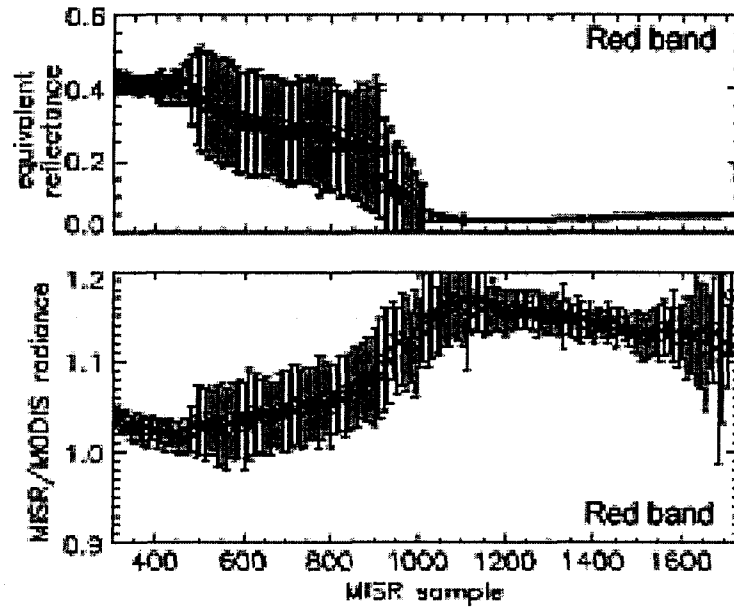


Figure 8. Top) Plot of mean equivalent reflectance across the Arabian Sea image shown in previous figure. The mean is calculated by averaging MISR radiances in the vertical (north-south) direction. Standard deviations around the mean are also shown. High standard deviations are where both land and water figure into the calculations. Bottom) Median MISR/ MODIS radiance ratio at each sample location, calculated by combining all points in the north-south direction. Standard deviations are also shown. Note the inconsistency between the ratio over water (dark scene) relative to land (bright scene).



Figure 9. High resolution Lunar image, Df\_Red channel.



Df\_Red



Df\_Green\_4x4

Figure 10. MISR viewed the moon in its baseline Global Mode configuration. Here twelve of the 36 MISR channels are configured to high-resolution (no averaging) during Global Mode, as shown in (a). Twenty four channels are in 4x4 pixel averaging mode, (b).



Df\_Red



Cf\_Red



Bf\_Red



Af\_Red

Figure 11. Lunar image resolution degrades in going from the D to A camera design, due to the smaller focal lengths in going from D to A..

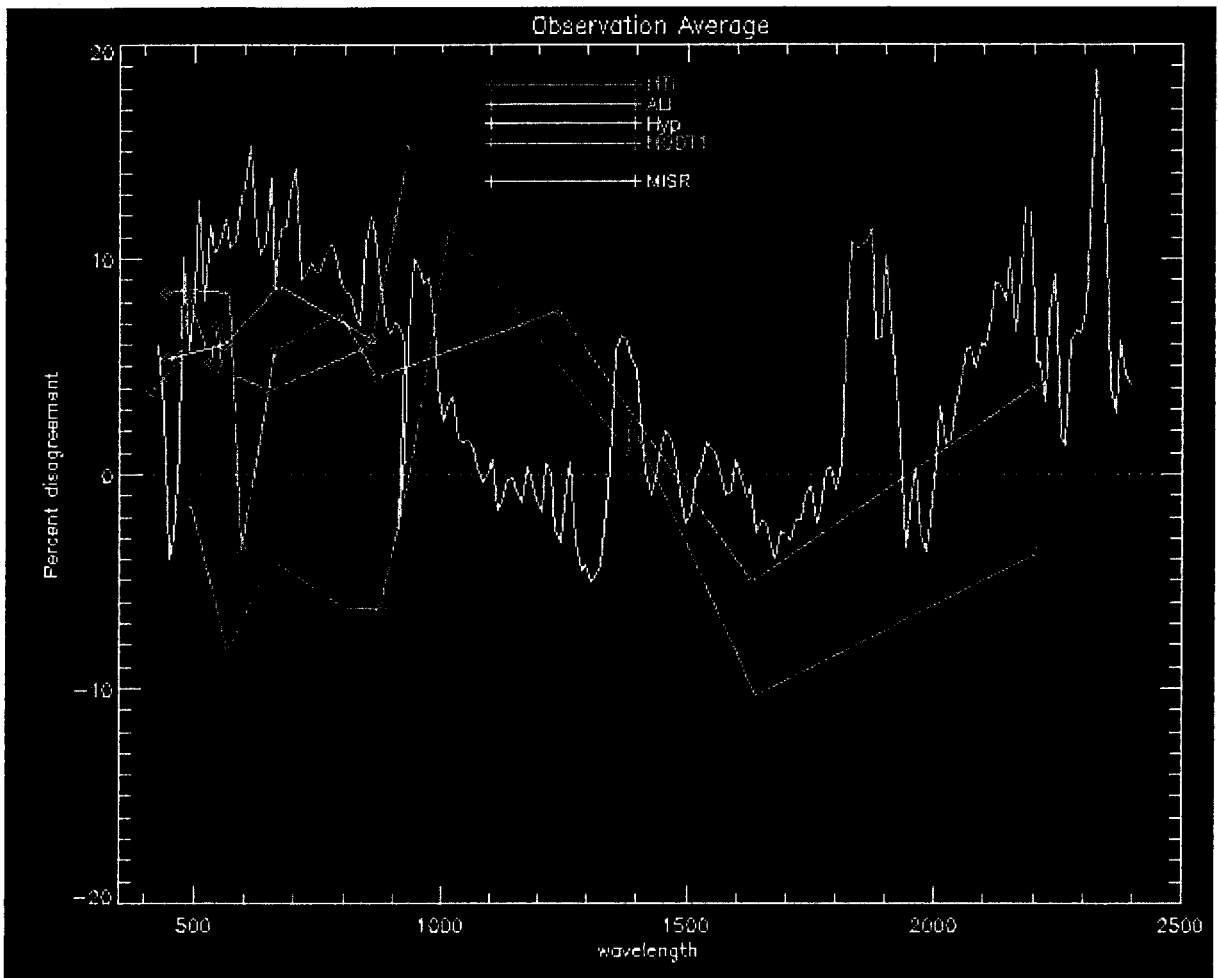


Figure 12. Differences between MISR and ROLO measure of lunar irradiance.